Received: 21 May 2020 | Revised: 1 August 2020 | Accepted: 15 September 2020

DOI: 10.1002/jccs.202000215

JOURNAL OF THE CHINESE CHEMICAL SOCIETY

ARTICLE

Design, synthesis, in silico analysis with PPAR-γ receptor and study of non-covalent interactions in unsymmetrical heterocyclic/phenyl fleximer

Ved Prakash Singh[1,2] | **Jayanta Dowarah**[1] | **Brilliant N. Marak**[1] | **Ashish Kumar Tewari**[2]

[1]Department of Chemistry, School of Physical Sciences, Mizoram University, Aizawl, Mizoram, India

[2]Department of Chemistry, Institute of Science, Banaras Hindu University, Varanasi, Uttar Pradesh, India

Correspondence
Ved Prakash Singh, Department of Chemistry, School of Physical Sciences, Mizoram University, Aizawl 796004, Mizoram, India and Department of Chemistry, Institute of Science, Banaras Hindu University, Varanasi-221 005, India.
Email: vpsingh@mzu.edu.in
Ashish kumar Tewari, Department of Chemistry, Institute of Science, Banaras Hindu University, Varanasi-221 005, India.
Email: tashish2002@yahoo.com

Funding information
Department of Science and Technology, Ministry of Science and Technology, India is the DST funding agency.

Abstract

This work deals with the design, synthesis, in silico analysis, crystallization, and the interpretation 2-cyano-3-{4-[2-(phthalimid-nyl)-propoxy]-phenyl}-acrylic acid ethyl ester (7). Analog 7 is designed based on rosiglitazone. The quantitative analysis of Compound 7 has been performed through single-crystal X-Ray Diffraction (XRD) and Hirshfeld surface analysis. Fleximer 7 has studied the role of flexibility in non-covalent interactions and binding affinity with PPAR-γ receptors. Both phthalimide ring and phenyl rings are linked with propylene linker. 2-cyano-3-{4-[2-(phthalimid-nyl)-propoxy]-phenyl}-acrylic acid ethyl ester has $Z = 8$ in the crystal packing and stabilized by inter-molecular non-covalent interactions like C—H...O, C—H...N, C—H...л, and л...л, and so forth.

KEYWORDS

crystal, docking, intra-molecular, fleximer, intermolecular, non-covalent interactions, PPAR-γ

1 | INTRODUCTION

Non-covalent interactions are of fundamental importance for understanding molecular recognition in biological systems,[1] and physical and chemical properties of new materials.[2–6] These play a vital role in influencing the assembly, conformation, and spacing of aromatic dimer stacks.[7–9] The understanding of the stack system about its orientation and spacing and control of these non-covalent forces in stabilizing the supramolecular self-assembly process is indispensable for the progress of crystal engineering.[10,11]

The acquisition of artificial nucleobases into DNA helix can lead the bio-chemist designer to study the natural systems.[12–18] Among various weak interactions, the facial stacking orientation of aromatic molecules are of particular interest as loan pair–π interactions. These interactions are intermolecular forces, which is very much similar to hydrogen bonding, whose nature is still undefined.[19] Arrangement of loan pair–π interactions between aromatic rings can generally be distinguished into two different situations: face-to-face, offset and slipped.[20]

A heterocyclic system is more favorable for aromatic interactions; for example, if nitrogen introduced or an electron-deficient ring is more prompt for aromatic interactions. Unsymmetrical fleximers having aromatic and heteroaromatic rings are studied like pyridines,[21] pyrazolo [3,4-d] pyrimidine, and so forth. Out of these studies, only a few have shown intra and inter-molecular stacking

interactions, whereas most of them show only intermolecular non-covalent aromatic interactions. Unsymmetrical dimer shows donor-acceptor type interactions of loan pair–π lateral offset stacking in imidazolin-5-ones. These studies show that how weak π···π interactions are exploited for tailoring supramolecular assemblies.[22] Consequently, to study the role of non-covalent interactions, we synthesized unsymmetrical flexible heterodimer, 2-cyano-3-{4-[2-(phthalimid-nyl)-propoxy]-phenyl}-acrylic acid ethyl ester (7) linked through methylene linkers.

The peroxisome proliferator-activated receptor belongs to the family of nuclear receptors.[23] Peroxisome proliferator-activated receptors (PPARs) are the group of nuclear receptors that control the carbohydrate metabolism by altering the expression of the genes involved. Rosiglitazone Thiazolidinedione (TZD) is an anti-diabetic drug of glitazone series. In general, the ligand is in a U-shaped conformation; the **TZD** head group makes several specific interactions with amino acids in H3, H4, H10, and the AF-2 helix.[24] The carbonyl groups of the TZD form hydrogen bonds with two histidine residues, H323 and H449. Y473 in the AF-2 helix forms a secondary hydrogen bond with H323. The partly negatively charged nitrogen of the TZD head group is within hydrogen-bonding distance of the Y473 side chain. A buried lysine residue, K367, forms another secondary hydrogen bond with rosiglitazone. Next to the head group, the sulfur atom of the TZD ring positioned in a hydrophobic region of the PPAR-γ. The central benzene ring of the ligand occupies a very narrow pocket between C285 and M364. The bridging oxygen atom between the benzene ring and the pyridine ring provides vital geometry for the pyridine ring, which occupies the pocket between H3 and the b-sheet. Substituted carboxylic acids can act as bio-isosteric replacements for the TZD head group, maintaining high-affinity binding and receptor activation.[24] All of these hydrophobic carboxylic acids may become the key to bind with PPAR. The main side effect of glitazones is water retention leading to edema, with significant water retention, leading to decompensation of potentially previously unrecognized heart failure. These side effects require the development of new molecules with potent anti-diabetic activities with the least side effects.

In the present work, compounds designed on the structural basis of rosiglitazone in Figure 1. In order to minimize the side effects of rosiglitazone, the head portion was replaced by one of its bio-isoester, dicarboxylic ester function. Cyano group was introduced to compensate for the nitrogen of TZD. Efforts were made to modify the tail portion of rosiglitazone by introducing phthalimide heterocyclic moieties rich in biological properties. The central benzene ring is retained as it is essential for anti-diabetic activities, confirmed from the crystal structure of rosiglitazone and its receptor PPARγ. Molecular recognition processes involving intermolecular interactions of compound and PPARγ are carried out by in-silico studies.

2 | RESULTS AND DISCUSSION

The compound crystallized in ethyl acetate: hexane solution at room temperature by the slow evaporation method. Only Z (7) isomer is obtained in the final step of the synthesis. This reaction takes place through a thermodynamically controlled product pathway because Z is thermodynamically more stable then E isomer.

2.1 | Crystal structure analysis

The compound is an unsymmetrical fleximer linked with a tri-methylene linker. One side of the dimer has phthalimide substituent, while the other side *p*-substituted phenyl ring is linked through oxygen atom (Table 1).

The phthalimide group selected for study due to its polarized nature exhibited both donors and an acceptor in intermolecular and intramolecular interactions. It is a polarized bicyclic system due to the amide group in one ring. Another part of the fleximer is a substituted phenyl ring, an electron-rich moiety of the compound. Oxygen linked to methylene linker and phenyl ring is also taking part in intra-molecular interaction, which creates a new conformation in molecules in the solid-state, and C18—C20 exists in gauche conformation.

The cyano group's nitrogen taking part in intra-molecular interaction with C13—H13 and angle of C7—C9—N10 becomes 178.43° in place of 180°. This C (13)—H(13)···N(10) weak bond forms seven-membered rings of C7, C8, C9, C10, C11, C13, N10, H13 atoms, which

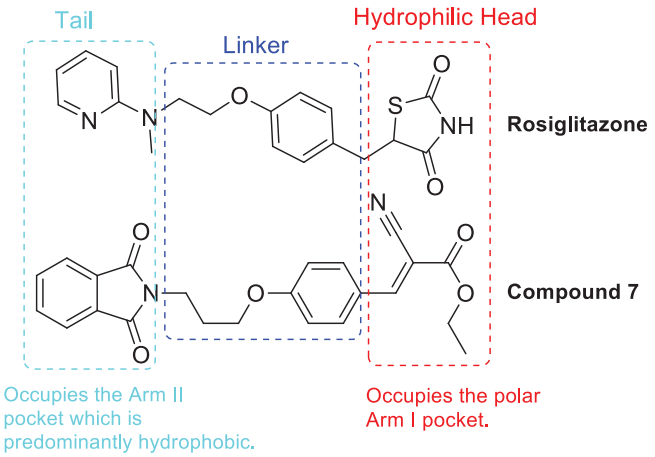

FIGURE 1 Similarity of Compound 7 with rosiglitazone

create an unsymmetrical bond angle between C8—C11—C13 and C8—C11—C12, which is 117.16° and 125.38°, respectively. O17 is involved in weak interactions with H19b. It is tilted toward C14, and the angle between O17—C16—C14 becomes 115.61°, whereas O17—C16—O15 becomes 124.81° in place of 120°. Intra-molecular interactions are summarized in Table 2 (Figure 2).

Crystal packing of molecules stabilized via various non-covalent interactions. In the packing diagram, four molecules arranged in two planes in two groups just perpendicular to the each other due to the presence of intermolecular edge to face C(29)—H(29)···π Cg(C26—C31) (3.130 Å), C(24)—O(25)···π Cg(N22, C23—C27) (2.407 Å), C(15)—H(15)···π Cg(C11—C16) (3.045 Å) interaction (Figure 3 and Table 3). These interactions are present between a similar ring of two molecules. Means five-membered ring interacts with a five-membered ring, and a six-membered ring interacts with a six-membered ring through loan pair interaction and C—H—л interactions.

Arene-arene interaction is also observed by expanding the crystal network, which stabilizes the unsymmetrical molecule in the opposite orientation, as observed in CH—π interactions. Aromatic loan pair–π interaction present between bicyclic phthalimide ring and phenyl ring Cg(C11—C16)π···πCg (N22, C23—C27) (3.448A°) (Figure 4 and Table 3).

There are two loan pair–π interactions between two molecules from both the ends of the molecule. These aromatic CH—π and loan pair–π interactions orient the molecules in opposite orientation into the ABAB pattern in Figure 5.

The Hirshfeld surface and fingerprint plots[27] of Compound 7 are in Figure 6. Hirshfeld surface view exactly explained the pattern of molecule conformation exists in

TABLE 1 Crystal data, data collection, and structure refinement for Compound 7 (CCDC 1907144)

Empirical formula	$C_{23}H_{20}N_2O_5$
Formula weight	404.42
Temperature	296 (2) K
Crystal system, space group	Monoclinic, $P2_1/c$
Unit cell dimensions	$a = 22.2055(6)$ Å, $\alpha = 90°$ $b = 11.0555(3)$ Å, $\beta = 91.312(2)°$ $c = 8.0619(2)$ Å, $\gamma = 90°$
Volume	1978.62(9) Å^3
Z	8
ρ_{calc}	1.3575 g/cm^3
μ	0.097 mm^{-1}
$F(000)$	848.5
Crystal size	0.35 × 0.30 × 0.25 mm
Radiation	Mo Kα ($\lambda = 0.71073$)
Index ranges	$-26 \le h \le 29$, $-13 \le k \le 12$, $-10 \le l \le 6$
Reflections collected	8,243
Independent reflections	4,440 [$R_{int} = 0.0168$, $R_{sigma} = 0.0365$]
Goodness-of-fit on F^2	0.954
Final R indexes [$I >= 2\sigma(I)$]	$R_1 = 0.0366$, $wR_2 = 0.0919$

Note: Computer programs: CrysAlis PRO, Oxford Diffraction Ltd., SHELXL2016/6[25] for first crystal, CrysAlis PRO, Oxford Diffraction Ltd., Version 1.171.33.41, olex2.solve,[26] olex2.refine.[26]

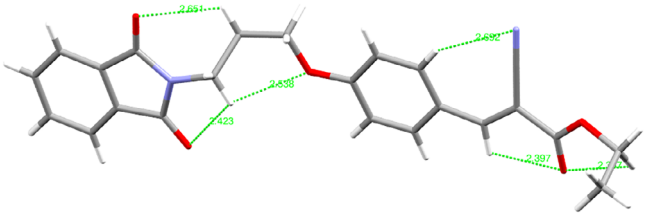

FIGURE 2 Intra-molecular interactions in Compound 7

TABLE 2 Intra-molecular interactions in Compound 7

S. No.	Interaction	d (Å)	D (Å)	C—H—N/O (°)
1.	C(19)—H(19b)···O(17)	2.513	2.914	104.61
2.	C(19)—H(19b)···O(21)	2.490	2.887	104.31
3.	C(20)—H(20b)···O(25)	2.656	3.172	113.66
4.	C(8)—H(8)···O(3)	2.406	2.803	105.60
5	C(2)—H(2a)···O(3)	2.407	2.688	96.03
6.	C(13)—H(13)···N(10)	2.696	3.523	148.52

the solid-state. Electronic distribution within the compound also explained the existence of non-covalent interactions (Figure 6). The principal weak interactions are visible in the fingerprint plots. The surface coverage for Compound 7 is H...H 39.8%, C...C 6.4%, N...H 7.7%, O...H 23.2%, C...H 16.1%, N...C 3.3%, C...O 3.1%, and other interactions are less than 0.2%. The primary intermolecular interactions are observable in the fingerprint plot. This study gives the exact contribution of different types of interactions like loan pair–π interaction contributes 6.4%, whereas CH-л interactions contribution is 16.1%.

The 2D fingerprint plots represent the weak intermolecular interactions with the pair of contacts and their percentage of contribution toward the 3D Hirshfeld surface formation. The di and de in the fingerprint plots represent the distance between the nearest internal element and external to the 3D molecular Hirshfeld surface, respectively.[28] The yellowish-red bin on the fingerprint plots also provided information about the presence of weak л–л stacking in the crystal structure (Figure 6b). The spoke-like pattern in the fingerprint plots represents the C—H...O interactions in the

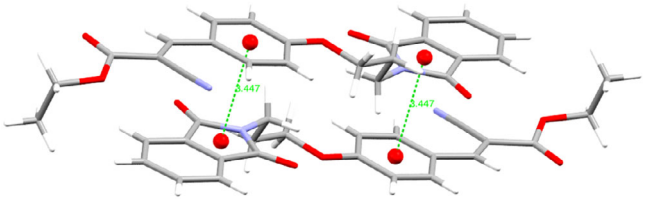

FIGURE 4 л...л interactions in the crystal of Compound 7

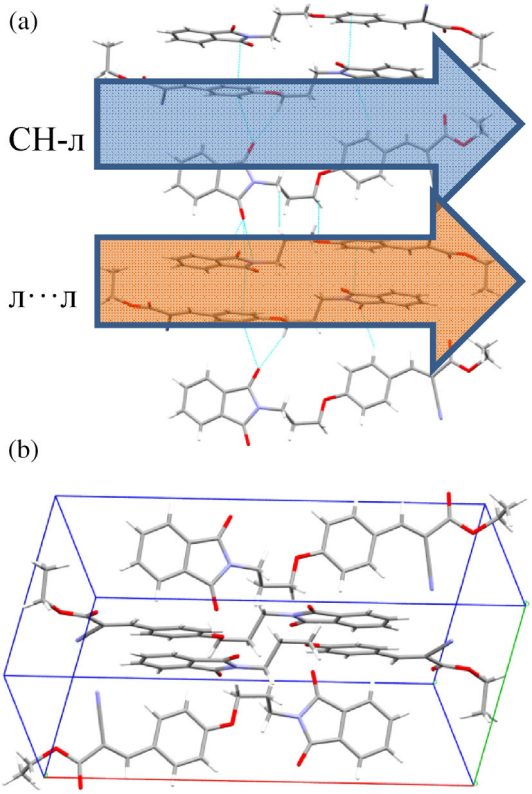

FIGURE 5 Crystal network (a) and unit cell packing (b) of Compound 7

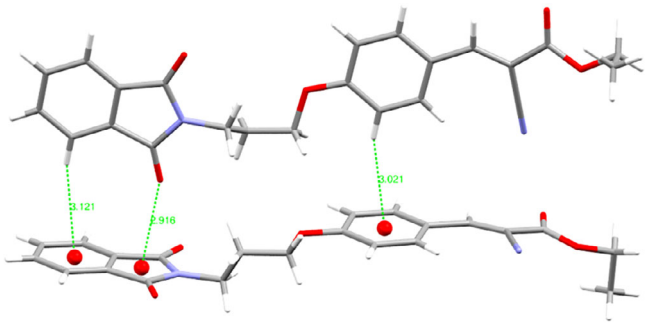

FIGURE 3 CH-л, loan pair-л interactions in Compound 7

TABLE 3 Intermolecular interactions in Compound 7

S. No.	Interaction	d (Å)	D (Å)	C—H—л/N/O (°)
1.	C(18)—H(18b)···O(21)	2.577	3.455	150.60
2.	C(12)—H(12)···O(25)	2.642	3.472	149.07
3.	C(18)—H(18a)···O(17)	2.662	3.281	122.06
4.	C(29)—H(29)···л Cg(C26—C31)	3.130	4.016	159.99
5	C(24)—O(25)···л Cg(N22, C23—C27)	2.407	4.030	152.40
6.	C(15)—H(15)···л Cg(C11—C16)	3.045	3.922	157.80
7.	Cg(C11—C16)л···лCg (N22, C23—C27)	3.448	—	—

crystal lattice in the region of di + de = 2.45–2.7 Å (Figure 6b). The C—H...л interactions can be seen as a pair of unique blue colored wings in the region of di + de = 2.45–2.7 Å(Figure 6b). The C—H...N pair of interactions of contacts also reflected as two characteristic wings occupied in the region of di + de = 2.45–2.7 Å (Figure 6b).

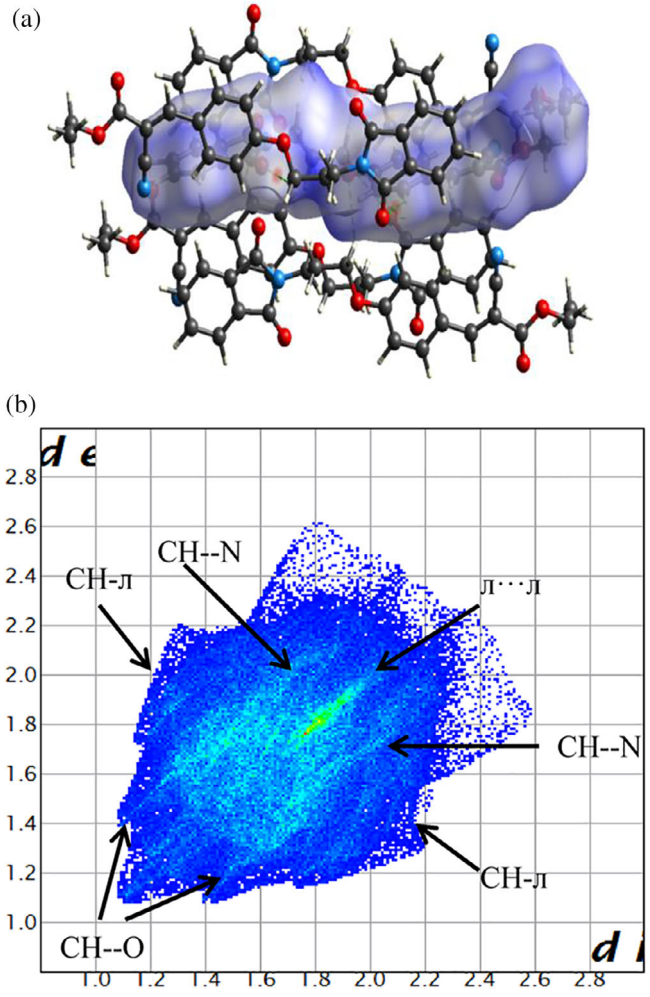

FIGURE 6 (a) Hirshfeld surfaces and (b) fingerprint plots of Compound 7

Calculated interaction energy with non-covalent interactions for Compound 7 is in Table 4. The Hirshfeld surface analysis also shows different kinds of weak non-covalent intermolecular interactions, where loan pair–π stacking, C—H...π interactions, C—H...N, and C—H...O interactions of Compound 7 in the crystal packing structure is in Figure 7. The dispersion component calculated for these interactions is the major component, presumably a result of the aromatic electronic re-distribution in the compound.[29] Another interaction of interest is these weak H-bonds (C—H...O and C—H...N), making a non-covalent interaction among neighbor molecules. There should be a significant electrostatic component, but the dispersion component is a major one found in this calculation, presumably a result of the charge distribution in the ester functional group and cyano group and the polarization of the phenyl ring by its substituents.

The Curvedness plots and the Shape index plots of 3D Hirshfeld also reveal the various weak intermolecular interactions in the crystal structure of Compound 7. The yellow spots in the Curvedness plots represent the weak interactions of Compound 7 in the crystal structure, shown in Figure 8a. The Curvedness plots also give information about the weak л-л stacking. The green-colored flat regions in the Curvedness plots indicate the presence of weak л-л stacking in the crystal structure of Compound 7.[29] The red-colored spots in Curvedness plots show strong hydrogen-bonding interactions in the crystal structure.

Red and blue areas represent the acceptor and the donor property, respectively, in shape index of Compound 7 (Figure 8b). Yellowish-red colored concave regions indicate the presence of weak intermolecular

TABLE 4 Interaction energies (kJ/mol) calculated for Compound 7

S. No.	D—H...A	E_ele	E_pol	E_dis	E_rep	E_tot
1	C1—H1b...N10, C1—H1b...O4,	−3.8	−1.4	−9.2	4.7	−10.2
2	C1—H1c...N10, C1—H1c...O4	−9.0	−3.5	−16.6	8.7	−21.2
3	C1—H1a...O3	1.1	−0.6	−7.4	1.2	−5.0
4	C2—H2a...O4, C2—H2a...O3	−1.8	−0.4	−9.1	1.8	−9.1
5		0.4	−0.6	−5.6	3.4	−2.8
6	C19—H19a...O17, C13—H13a...C26C27C28C29C31C0aa, C11C12C13C14C15C16...C23C24C26C27N22	−28.3	−3.6	−127.1	76.5	−96.0
7	C15—H15...C11C12C13C14C15C16	−12.9	−8.9	−62.6	43.2	−48.0
8	C12—H12...O25, C18-H18b...O21	−25.3	−6.7	−44.4	31.6	−50.9
9	C12—H12...O21, C14—H14...O21, C0aa—H0aa...O3, C12-H12...C23, C12—H12...C26	−8.5	−3.9	−44.7	25.4	−35.1

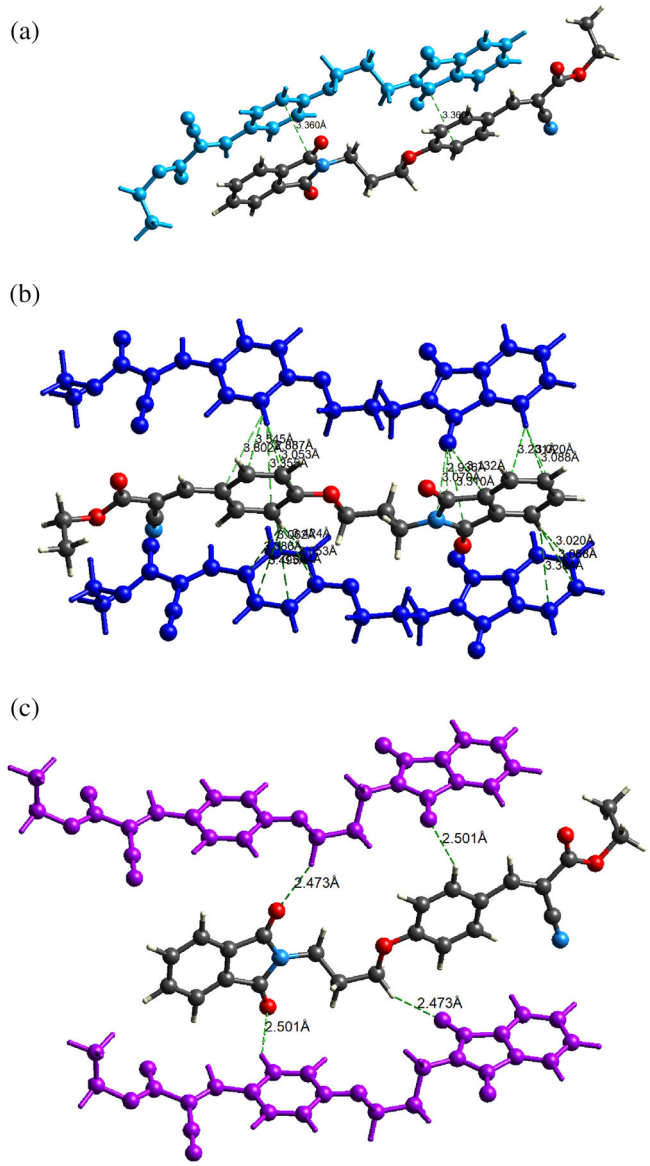

FIGURE 7 (a) л-л stacking, (b) C—H...л interactions, (c) C—H...O interactions of Compound 7 in Hirshfeld surface analysis

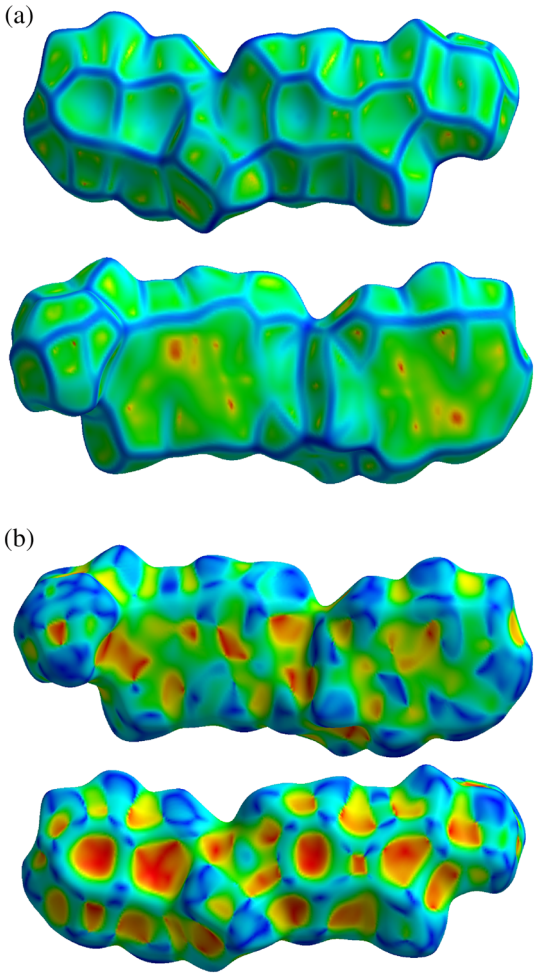

FIGURE 8 (a) curvedness both side view, (b) shape index both side view of Compound 7

interactions in the Shape index plots.[30,31] The red and blue colored triangles on the surface of rings of the molecule in the Shape index plots also indicated the presence of weak л–л stacking in the crystal structure (Figure 8b). Hirshfeld surface analysis gives evidence about weak intermolecular interactions, and all these weak interactions stabilize and strengthen the crystal packing structure of Compound 7.

2.2 | In silico analysis

The ligand-binding pocket of PPAR-γ has a sizable Y-shaped cavity. It is comprised of three sub-pockets viz. Arm I, Arm II, and Arm III. Arm-I is mostly polar, and it is located near H12; Arm II contains some polar residues. However, it is predominantly hydrophobic and lies close to the β-sheet of the surface. Whereas, the Arm III pocket is also hydrophobic and located near the β-sheet but buried deeper near H5.[32] Compound 7 binds with PPAR-γ receptor through C—H...O, C—H...N, C—H...π, and π...π non-covalent interactions in the same way as observed in crystal analysis and Hirshfeld analysis. The donor and acceptor region of crystal structure and Hirshfeld analysis found similar as observed in the binding of Compound 7 with PPAR-γ receptor in docking analysis.

The binding mode of Compound 7 in the active site of PPAR-γ was examined in depth using molecular docking analysis. The analysis of docking results indicated that Compound 7 has a high binding affinity in the active site of PPAR-γ. It has a binding energy of 9.3 kcal/mol, higher than the binding energy of rosiglitazone (8.3 kcal/mol). Much like rosiglitazone, Compound 7 occupied Arm I and Arm II of the ligand-binding pocket, and the arm-III pocket remains unoccupied. The three-dimensional representation

of Compound 7 in the binding cavity of PPAR-γ is illustrated in Figure 9. The more hydrophilic group of Compound 7, that is, ethyl cyanoacrylate, occupied the most polar pocket Arm I, whereas less polar group phthalimide directed toward the Arm II pocket. The ethyl cyanoacrylate established two strong hydrogen bonds with the residues Ser289 and Tyr327 in the Arm I pocket. In contrast, the carbonyl oxygen of phthalimide exhibited one hydrogen bond interaction with the residue Ser342 in the Arm II pocket. In addition to hydrogen bond interactions, π-sulfur interactions with the residues Cys285 and Met364, and π-alkyl interactions with the residues Phe282, His499, Ile341, Cys285, Arg288, and Leu330 largely contributed to its binding affinity in the ligand-binding domain of PPAR-γ.

3 | EXPERIMENTAL

3.1 | Synthesis of 2-cyano-3-{4-[2-(phthalimid-nyl)-propoxy]-phenyl}-acrylic acid ethyl ester (7)

In a 100 ml round bottom flask 4-(3-phthalimid-nyl-propoxy) benzaldehyde (0.32 g, 1.02 mmol), ethyl cyano acetic acid ethyl ester (0.1153 g, 1.02 mmol), piperidine (0.005 g), and sodium acetate (0.008 g) were taken in toluene. Flask was attached to the dean stark apparatus. The reaction mixture refluxed for 7 hr. Completion of the reaction was monitored through thin layer chromatography. The solvent was evaporated, and the residue was extracted with chloroform (3 × 200 ml) and washed with water (3 × 100 ml). The combined organic layer was dried by anhydrous sodium sulfate. Chloroform was evaporated, and crude was purified through column chromatography using ethyl acetate and hexane as eluent. Pure compound was collected from 22% EtOAc/Hexane, followed by recrystallization in ethyl acetate and hexane. Single crystal X-ray Ortep diagram of this compound confirms that these reactions gave Z-isomer only (Scheme 1).

3.1.1 | 1HNMR 300 MHz, 25oC, Si(CH3)4, (CDCl3), δ (ppm)

1.37–1.41 (3H, t, CH3, J = 6.9 Hz, J = 7.2 Hz); 2.21–2.25 (2H, m, CH2); 3.90–3.95 (2H, t, NCH2, J = 6.6 Hz, J = 6.6 Hz); 4.01–4.14 (2H, t, OCH2, J = 5.7 Hz, J = 6.0 Hz); 4.33–4.39 (2H, q, CH2); 6.85–6.88 (2H, d, ArH, J = 8.7 Hz); 7.93–7.96 (2H, d, ArH, J = 8.7 Hz); 7.71–7.85 (4H, m, ArH); 8.15 (1H, s, C═C—H). 13C NMR (75 MHz, CDCl3): (δ): 14.09, 27.97, 35.16, 62.29, 66.02, 99.18, 114.97, 116.07, 123.15, 124.27, 131.93, 133.47, 133.93, 154.22, 162.76, 162.96, 168.20.

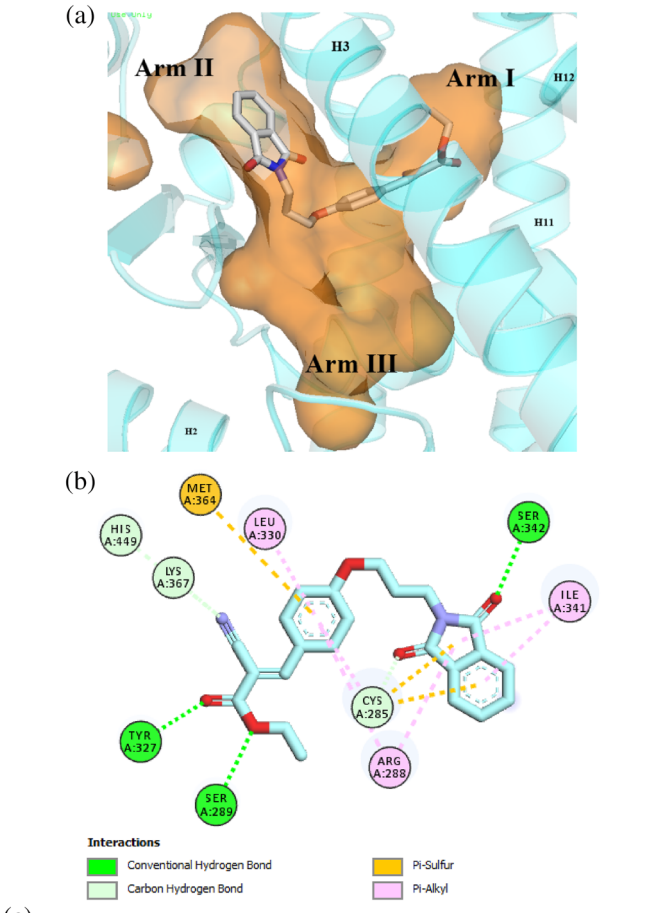

FIGURE 9 Illustrations of the binding mode of Compound 7 in the ligand-binding domain of PPAR-γ. (a) The Y-shaped cavity of the ligand-binding domain. (b) Molecular interactions of Compound 7 with PPAR-γ. (c) Overlay of Compound 7 with rosiglitazone

3.2 | Crystal structure determinations

Single-crystal X-ray data for compounds 7 was collected with an Oxford Diffraction Xcalibur CCD diffractometer. Graphite monochromated Mo Kα (λ = 0.71073 Å) was used as a radiation source. The structures were determined by direct methods using Olex-2.[25] It is refined on F2 by a full-matrix least-squares technique.[25,26] Non-hydrogen atoms were refined anisotropically, and hydrogen atoms were geometrically fixed with thermal parameters equivalent to 1.2 times that of the atom to which

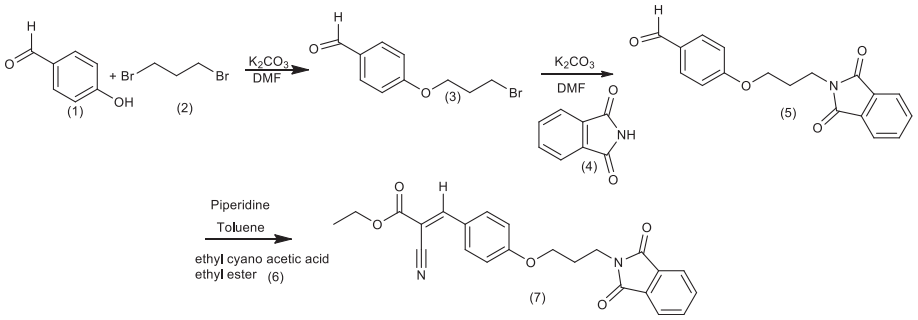

SCHEME 1 (7); Yield: 0.39 g, 94%. M.p.: 129–132°C

they bonded. All diagrams of the compounds were prepared using Oak Ridge Thermal Ellipsoid Plot, and the packing diagrams were generated using Mercury version 3.1.[33a] Ortep and Mercury were used to analyze bond lengths, bond angles, and other geometrical parameters.[33b]

3.3 | Hirshfeld surface and fingerprint plots analysis

Hirshfeld surfaces, fingerprint plots, interaction energies, and energy frameworks were calculated using CrystalExplorer17.5.[34] The interactions energy calculations also showed sufficient evidence about the different kind of weak intermolecular interactions. The interaction energies of Compound 7 calculated using the CE-B3LYP/6-31G(d,p) functional/basis set combination.[35] The interaction energy is broken down as

$$Etot = keleE'ele + kpolE'pol + kdisE'dis + krepE'rep \quad (1)$$

where the *k* values are scale factors, E′ele represents the electrostatic component, E′pol the polarization energy, E′dis the dispersion energy, and E′rep the exchange-repulsion energy.[36]

3.4 | Molecular docking

Molecular docking analysis was carried using the autodockVina.[37] It involves a series of steps like protein selection from a protein data bank and its preparation, grid generation, ligand preparation, and docking to the receptor. PPAR-γ protein for docking retrieved from the protein data bank (PDB id: 5YCP). The protein preparation was done in chimera[38] by deleting co-crystallized ligand and embedded water molecules. It was further processed by adding polar hydrogens and assigning partial charges. The grid was generated to cover the ligand-biding domain of PPAR-γ, and the exhaustiveness parameter for analyzing the binding affinity. It was set to nine modes. Finally, the processed protein structure subjected to docking with the crystal structure of Compound 7. The docked results were visualized using the pymol and Discovery Studio.[39,40]

4 | CONCLUSIONS

Cyano-3-{4-[2-(phthalimid-nyl)-propoxy]-phenyl}-acrylic acid ethyl ester is a thermodynamically controlled product Z isomer formed as a product. Crystal packing and its network have stabilized by different types of intramolecular interactions (C—H...O, C—H...N), and intermolecular (C—H...O, C—H...π, and π...π) non-covalent interactions. Non-covalent interactions orient the molecule in opposite orientation in the solid-state due to charge dispersion, polarization, and charge re-orientation of conjugated π electrons. Charge re-organization due to the neighbor molecule is very similar in the crystal structure, Hirshfeld surface analysis, and in the drug-receptor analysis. The polarization of molecules defines the orientation of molecules in the solid-state, taking part in drug-receptor binding, as observed in docking analysis. Crystal property can be utilized in the development of a new drug by using its donor-receptor property. The flexibility of Compound 7 gives a better conformation to fit the Y-shaped cavity of the PPAR-γ receptor. Flexibility enhances the selectivity and binding affinity of analogs. This Compound 7 shows a potentially binding affinity toward the PPAR-γ receptor even better than then rosiglitazone standard drug. This compound maybe becomes a better anti-diabetic drug as per docking analysis. This Compound 7 can be further in vivo studied to develop a new anti-diabetic drug.

ACKNOWLEDGMENTS

Department of Chemistry, Banaras Hindu University, Varanasi, INDIA is acknowledged for departmental facilities. Department of Chemistry, Mizoram University, Aizawl, Mizoram, India, acknowledged the other infrastructure facilities. The author Jayanta Dowarah acknowledged DST for Inspire fellowship for financial support.

CONFLICT OF INTEREST

The authors declare no potential conflict of interest.

ORCID

Ved Prakash Singh https://orcid.org/0000-0003-4401-8379

REFERENCES

[1] (i) V. P. Singh, *Sci. Technol. J.* **2015**, *3*(1), 42; (ii) A. K. Tewari, P. Srivastava, V. P. Singh, P. Singh, R. S. Khanna, *Res. Chem. Intermed.* **2013**, *39*(7), 2925.
[2] G. R. Desiraju, *Crys. Eng. Des. Org. Solids*. Elsevier Science Publishers B. V., Amsterdam **1989**.
[3] C. A. Hunter, J. K. M. Saunders, *J. Am. Chem. Soc.* **1990**, *112*, 5525.
[4] D. K. Muller, P. Hobza, *Chem. Rev.* **2000**, *100*, 143.
[5] G. R. Desiraju, T. Steiner, *Weak Hyd. Bond Struc. Chem. Bio.* Oxford University Press, Oxford **2000**.
[6] T. Steiner, *Angew. Chem., Int.* **2002**, *41*, 48.
[7] A. N. Sokolov, T. Friščic, L. R. MacGillivray, *J. Am. Chem. Soc.* **2006**, *128*, 2806.
[8] T. Seki, S. Yagai, T. Karatsu, A. Kitamura, *J. Org. Chem.* **2008**, *73*, 3328.
[9] K. Katagiri, T. Tohaya, H. Masu, M. Tominaga, I. Azumaya, *J. Org. Chem.* **2009**, *74*, 2804.
[10] B. W. Gung, X. W. Xue, H. J. Reich, *J. Org. Chem.* **2005**, *70*(9), 3641.
[11] A. K. Tewari, V. P. Singh, C. Puerta, P. Valerga, *Acta Cryst.* **2007**, *E63*, 1930.
[12] O. Baudoin, F. Gonnet, M. P. Teulade-Fichou, J. P. Vigneron, J. C. Tabet, J. M. Lehn, *Chem. A-Eur.* **1999**, *J5*, 2762.
[13] T. Benzing, T. Tjivikua, J. Wolfe, J. Rebek, *Science.* **1988**, *242*, 266.
[14] M. Sirish, H. J. Schneider, *J. Am. Chem. Soc.* **2000**, *122*, 5881.
[15] S. R. Waldvogel, R. FrThlich, C. A. Schalley, *Angew. Chem.* **2000**, *112*, 2580.
[16] J. N. Wilson, E. T. Kool, *Org. Biomol. Chem.* **2006**, *4*, 4265.
[17] A. T. Kruger, L. Haige, A. H. F. Lee, E. T. Kool, *Acc. Chem. Res.* **2007**, *40*, 141.
[18] P. G. A. Janssen, S. Jabbari-Farouji, M. Surin, X. Vila, J. Gielen, T. F. A. de Greef, M. R. J. Vos, P. Bomans, N. A. J. M. Sommerdijk, P. C. M. Christianen, P. Leclère, R. Lazzaroni, P. van der Schoot, E. W. Meijer, A. P. H. J. Schenning, *J. Am. Chem.* **2009**, *131*, 1222.
[19] C. A. Hunter, *Chem. Soc. Rev.* **1994**, *23*, 101.
[20] S. Tsuzuki, *Struct. Bond. (Berlin)* **2005**, *115*, 149.
[21] F. N. Khan, S. M. Roopan, V. R. Hathwar, M. Akkurt, *Acta Cryst.* **2010**, *E66*, 1001.
[22] B. K. Rajbongshi, G. Ramanathan, *J. Chem. Sci.* **2009**, *121*, 973.
[23] V. P. Singh, *Sci. Tech. J.* **2016**, *4*, 113.
[24] J. Dowarah, V. P. Singh, *Bioorg. Med. Chem.* **2020**, *28*(5), 115263(1–78). https://doi.org/10.1016/j.bmc.2019.115263.
[25] G. M. Sheldrick, *Acta Crystallog.* **2008**, *A64*, 112.
[26] O. V. Dolomanovn, L. J. Bourhis, R. J. Gildea, J. A. K. Howard, H. Puschmann, *J. Appl. Cryst.* **2009**, *42*, 339.
[27] C. F. Mackenzie, P. R. Spackman, D. Jayatilaka, M. A. Spackman, *IUCrJ.* **2017**, *4*, 575.
[28] J. J. McKinnon, M. A. Spackman, A. S. Mitchell, *Acta Crystallogr.* **2004**, *B60*, 627.
[29] V. P. Singh, J. Dowarah, D. K. G. Lalhruaizela, *Cryst. Res. Technol.* **2019**, *55*, 1900136(1–7).
[30] S. Shyamapada, M. Christoph, M. Samiran, *Acta. Chim. Slov.* **2016**, *63*, 129.
[31] K. M. Rahul, K. J. Amanpreet, A. Meenu, K. C. Sukhvinder, *J. Chem. Sci.* **2015**, *127*, 849.
[32] J. Shang, R. Brust, S. A. Mosure, J. Bass, P. Munoz-Tello, H. Lin, T. S. Hughes, M. Tang, Q. Ge, T. M. Kamenekca, D. J. Kojetin, *Elife* **2018**, *7*, e43320(1–34). https://doi.org/10.7554/eLife.43320.
[33] (a)I. J. Bruno, J. C. Cole, P. R. Edgington, M. K. Kessler, C. F. Macrae, P. McCabe, J. Pearson, R. Taylor, *Acta Cryst.* **2002**, *B58*, 389. (b) L. J. Farrugia, *J. Appl. Cryst.* **2012**, *45*, 849.
[34] J. J. McKinnon, M. A. Spackman, A. S. Mitchell, *Acta-Crystallogr* **2004**, *B60*, 627.
[35] S. F. Boys, F. Bernardi, *Mol. Phys.* **1970**, *19*, 553.
[36] M. J. Turner, S. Grabowsky, D. Jayatilaka, M. A. Spackman, *J. Phys. Chem. Lett.* **2014**, *5*, 4249.
[37] O. Trott, A. J. Olson, *J. Comput. Chem.* **2010**, *31*, 455. https://doi.org/10.1002/jcc.21334.
[38] E. F. Pettersen, T. D. Goddard, C. C. Huang, G. S. Couch, D. M. Greenblatt, E. C. Meng, T. E. Ferrin, *J. Comput. Chem.* **2004**, *25*, 1605.
[39] W. L. DeLano, *The PyMOL Molecular Graphics System*, Delano Scientific, San Carlos, CA **2002**.
[40] *Accelrys Discovery Studio Visualizer v 3.5*, Accelrys Software Inc, San Diego, CA **2010**. http://www.accelrys.com.

SUPPORTING INFORMATION

Additional supporting information may be found online in the Supporting Information section at the end of this article.

How to cite this article: Singh VP, Dowarah J, Marak BN, Tewari AK. Design, synthesis, in silico analysis with PPAR-γ receptor and study of non-covalent interactions in unsymmetrical heterocyclic/phenyl fleximer. *J Chin Chem Soc*. 2020;1–9. https://doi.org/10.1002/jccs.202000215